

# Cold Neutron Imaging and Efficiency Measurements with a Boron-10 Coated Double-GEM Detector

WooJong Kim<sup>‡</sup>    DongHyun Kim<sup>1</sup>    Minjae Kwon<sup>3</sup>  
Jason Sang Hun Lee<sup>1</sup>    Hyupwoo Lee<sup>1</sup>    Inkyu Park<sup>1</sup>  
Donghyun Song<sup>1</sup>    Inseok Yoon<sup>2</sup>    Myeonghun Choi<sup>1</sup>

<sup>1</sup>Department of Physics, University of Seoul, Republic of Korea

<sup>2</sup>Institute of Basic Sciences, Seoul National University, Republic of Korea

<sup>3</sup>Department of Physics, University of Turin, Italy

## Abstract

A  $^{10}\text{B}$ -coated GEM neutron detector (BGEM) was developed as a  $^3\text{He}$ -free alternative for cold-neutron beamline instrumentation, employing a single  $\text{B}_4\text{C}$  converter cathode, a double-GEM amplification stage, and an orthogonal strip readout over an active area of  $10 \times 10 \text{ cm}^2$ . Performance was evaluated at the Bio-REF cold-neutron beamline of the HANARO research reactor using a monochromatic  $4.5 \text{ \AA}$  beam ( $E_n = 4.03 \text{ meV}$ ). The absolute detection efficiency, measured relative to a calibrated  $^6\text{Li}$ -based Ce:LiCAF scintillation detector, was  $\varepsilon_{\text{BGEM}} = 8.69 \pm 0.20 \%$  (stat.). The spatial resolution was estimated from the edge smearing of reconstructed images of  $1 \text{ mm}$  diameter Cd-mask holes via an error-function fit to the radial edge profile, yielding approximately  $700 \mu\text{m}$ . These results demonstrate stable cold-neutron operation of a single-converter BGEM detector and provide a baseline for further efficiency improvements via converter and geometry optimization.

---

\*Corresponding author: kwj1180@uos.ac.kr

**Keywords:** Cold neutron detection; Boron-10 carbide converter; Gas Electron Multiplier (GEM);  $^3\text{He}$ -free detector; Detection efficiency; Spatial resolution

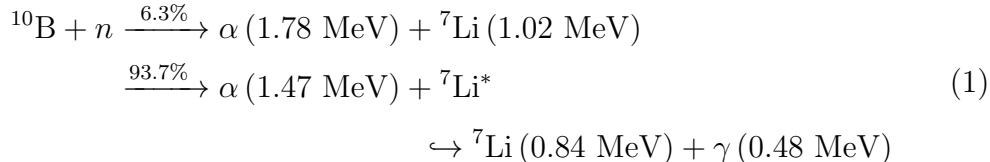
## 1 Introduction

Neutron detection technology plays a pivotal role in diverse applications, ranging from neutron diagnostics in nuclear fusion and boron neutron capture therapy (BNCT)[1] to process monitoring in nuclear fuel cycle technologies, such as pyroprocessing[2]. Consequently, the demand for cost-effective and high-performance neutron detection systems is steadily increasing across these domains.

Since neutrons carry no electric charge, their detection relies on secondary charged particles generated via scattering or nuclear capture reactions. Unlike direct ionization detectors used for charged particles or gamma rays, neutron detectors require a specific neutron-reactive converter material. Historically, standard detectors have employed  $^3\text{He}$  or, more recently,  $^6\text{Li}$  as converter materials. While  $^3\text{He}$  gas offers high detection efficiency, it is a strategic resource facing severe supply shortages [3]. Alternatively,  $^6\text{Li}$  is a viable option; however, the intrinsic properties of its crystal form present significant challenges for large-area detector fabrication. Consequently, we investigated alternative materials with high neutron capture cross-sections to develop a robust and scalable neutron detector.

Materials such as  $^{157}\text{Gd}$  and  $^{10}\text{B}$  are recognized as viable alternatives to  $^3\text{He}$  due to their large neutron capture cross-sections [4]. Although  $^{157}\text{Gd}$  exhibits a high capture probability, it emits low-energy internal conversion electrons, which complicates the discrimination of neutron signals from gamma-ray backgrounds [5]. Therefore, this study utilizes  $^{10}\text{B}$  due to its superior signal characteristics. As illustrated in Eq. 1, upon neutron absorption,  $^{10}\text{B}$  undergoes the  $^{10}\text{B}(n, \alpha)^7\text{Li}$  reaction, producing energetic alpha and lithium ions, often accompanied by gamma emission [6]. The high Q-value of this reaction ensures the generation of large ionization signals, facilitating robust

neutron detection. Furthermore, the cost-effectiveness of boron supports the scalability required for manufacturing large-area detectors.



To realize a large-area detector cost-effectively, we adopted the Gas Electron Multiplier (GEM) technology [7]. The GEM was selected not only for its scalability and economic viability but also for its excellent spatial resolution. Furthermore, its extensive research history and demonstrated reliability in various experimental conditions provide a solid foundation for this study. In this paper, we present the design and performance of a  ${}^{10}\text{B}$ -coated GEM, hereafter referred to as the BGEM detector.

## 2 Detector Design and Fabrication

### 2.1 Geometry Optimization via Geant4 Simulation

In this study, GEANT4 [8] simulations were performed to optimize the detector geometry and validate the feasibility of the concept. First, we evaluated various coating configurations for the boron-10 carbide ( ${}^{10}\text{B}_4\text{C}$ ) converter. While coating directly on the GEM foils was considered to potentially enhance detection efficiency, it was excluded from the final design due to concerns regarding negative impacts on high-voltage stability. Consequently, a configuration utilizing a  ${}^{10}\text{B}_4\text{C}$ -coated cathode was selected as the optimal baseline.

The simulation also focused on optimizing the drift gap length to maximize the signal amplitude. The drift gap was determined based on the stopping range of the secondary charged particles, particularly the alpha particles generated from neutron capture. The results indicated that a drift gap of 10 mm is sufficient to fully contain the alpha particle tracks, thereby maximizing the total energy deposition within the drift volume.

Finally, the simulation framework served as a theoretical baseline for understanding the detector’s operational characteristics. By comparing the simulated detection efficiency and pulse height spectra with experimental data, we could perform a robust cross-check of the detector’s performance and validate the measured efficiency.

Further details regarding the simulation setup can be found in [9].

## 2.2 Detector Fabrication

Guided by the simulation results indicating the optimal geometry, we developed a BGEM detector to validate the design under cold-neutron irradiation. For the neutron converter, a 1.5  $\mu\text{m}$  thick layer of  $^{10}\text{B}_4\text{C}$  was coated onto the cathode. Fig. 1 shows the  $^{10}\text{B}_4\text{C}$  coated cathode. Although the study [10] suggests that a coating thickness of approximately 3  $\mu\text{m}$  yields higher detection efficiency, we selected a thickness of 1.5  $\mu\text{m}$  to prioritize mechanical stability and mitigate the risks of film peeling or delamination, which are often associated with thicker coatings.

Strict quality control was maintained during deposition to minimize boron nitride (BN) formation arising from residual nitrogen in the chamber. The formation of BN impurities lowers the effective atomic density of  $^{10}\text{B}$  within the converter. This inevitably reduces the macroscopic absorption cross-section and the resulting neutron capture probability. The coating quality was primarily evaluated by visual inspection of the surface luster. A high-quality  $^{10}\text{B}_4\text{C}$  layer shows a characteristic metallic sheen, whereas BN-contaminated coatings typically appear translucent or whitish. All cathode foils used in this work exhibited the metallic sheen consistent with a  $^{10}\text{B}_4\text{C}$ -rich coating (Fig. 1).

The amplification stage employs  $10 \times 10 \text{ cm}^2$  GEM foils, which were produced at the facility described in Ref. [11]. This ensures that the manufacturing conditions and quality control adhered to established standards. Each foil consists of a 50  $\mu\text{m}$  thick polyimide substrate clad on both sides with 5  $\mu\text{m}$  thick copper layers. The foils feature standard biconical holes with outer and inner diameters of 70  $\mu\text{m}$  and 50  $\mu\text{m}$ , respectively, arranged in a hexagonal



**Figure 1:** Photograph of the cathode foil coated with  $1.5\ \mu\text{m}$  of  $^{10}\text{B}_4\text{C}$ . The distinct reflection of the photographer’s hand and camera on the surface serves as evidence of the mirror-like finish, confirming the high quality of the metallic coating and the absence of non-reflective impurities.

pattern with a pitch of  $140\ \mu\text{m}$ .

To verify that the detected signals originate from neutron capture reactions in the boron layer, we prepared two identical detector setups: one equipped with the  $^{10}\text{B}_4\text{C}$ -coated cathode and a reference detector without the coating. By comparing the response of these two detectors under the same beam conditions, we could confirm the neutron sensitivity attributed specifically to the  $^{10}\text{B}_4\text{C}$  layer.

The signal readout is provided by an orthogonal strip anode with 256 strips along the X-axis and 256 strips along the Y-axis, resulting in a total of 512 readout channels. For signal acquisition, custom-made readout electronics based on the APV25 ASIC [12] were employed.

### 3 Experimental Setup and Method

To evaluate the neutron detection performance of the fabricated prototype, beam tests were conducted at the Bio-REF cold neutron beamline of the HANARO (High-flux Advanced Neutron Application ReactOr) facility[13].

During the experiment, the reactor operated at a thermal power of 27 MW. The Bio-REF beamline delivers a monochromatic cold neutron beam with a mean energy of approximately 4.03 meV ( $\lambda = 4.5 \text{ \AA}$ ) and a maximum neutron flux of  $4.8 \times 10^6 \text{ n/cm}^2/\text{s}$ . The incident beam profile was defined by a  $\text{B}_4\text{C}$  slit, resulting in a beam size of 40 mm (horizontal)  $\times$  0.2 mm (vertical).

The trigger signal was derived from the bottom copper layer of the second GEM foil via AC coupling. The signal was first processed by an ORTEC 142PC charge-sensitive preamplifier. Subsequently, pulse shaping and amplification were performed using an ORTEC 474 timing filter amplifier to optimize the signal for triggering.

We performed a comparative study of the count rates from both the coated and uncoated detectors as a function of the applied voltage. Measurements were acquired under both beam-on and beam-off conditions. This approach allowed us to evaluate the dependence of neutron detection efficiency on the detector gain and to quantify the specific contribution of the boron coating to the total event rate.

### 3.1 Absolute Efficiency Measurement Setup

The absolute detection efficiency was evaluated using a Ce:LiCAF scintillator as a reference detector. The efficiency of the boron-coated GEM ( $\epsilon_{\text{BGEM}}$ ) was determined by comparing its background-subtracted count rate to that of the reference detector under identical beam conditions, as defined by Eq. 2:

$$\epsilon_{\text{BGEM}} = \frac{(R_{\text{BGEM, on}} - R_{\text{BGEM, off}})}{(R_{\text{LiCAF, on}} - R_{\text{LiCAF, off}})} \times \epsilon_{\text{LiCAF}} \quad (2)$$

, where  $R_{\text{BGEM, on}}$  and  $R_{\text{BGEM, off}}$  denote the measured count rates of the boron-coated GEM detector under beam-on and beam-off conditions, respectively. Similarly,  $R_{\text{LiCAF, on}}$  and  $R_{\text{LiCAF, off}}$  represent the corresponding count rates obtained from the reference Ce:LiCAF scintillator under the same experimental conditions. The term  $\epsilon_{\text{LiCAF}}$  refers to the intrinsic detection efficiency of the reference detector.

While previous studies regarding a 2 mm thick Ce:LiCAF scintillator reported a relative efficiency of  $82 \pm 5\%$  compared to a GS20 glass [14], we

assumed an intrinsic efficiency of unity ( $\epsilon_{\text{LiCAF}} \approx 1$ ) for the reference detector used in this study. This assumption is justified by two factors. First, the incident beam consisted of cold neutrons (4.03 meV), which have a significantly higher capture cross-section of  ${}^6\text{Li}$  compared to thermal neutrons due to the  $1/v$  dependence. Second, the scintillator used in our setup had a thickness of 10 mm, which is sufficiently thick to act as a total absorber for the cold neutron beam, effectively mitigating the transmission losses observed in thinner samples described in the literature.

## 4 Results

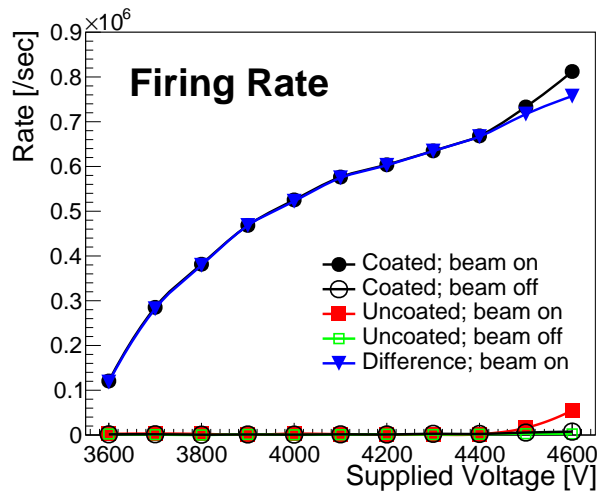


**Figure 2:** Measured event rates as a function of applied high voltage for both the boron-coated and uncoated detectors under beam-on and beam-off conditions. The curve labeled “Difference” represents the count rate of the coated detector minus that of the uncoated detector, illustrating the net neutron capture signal.

The successful detection of neutrons was first confirmed by the event rate measurements. Fig. 2 compares the count rates of the boron-coated and uncoated detectors as a function of the applied voltage under both beam-on and beam-off conditions. In the beam-off state, both configurations yielded neg-

ligible background counts, demonstrating that the electronic noise level remains low despite the low discrimination threshold. Under beam irradiation, only the boron-coated detector exhibited a substantial increase in event rate, characteristic of neutron capture signals. The uncoated detector showed a minor response only at voltages exceeding 4500 V, which is likely attributable to 478 keV prompt gamma rays originating from neutron absorption in the  $B_4C$  beam-defining slit. These results confirm that the signal observed in the coated detector is predominantly driven by neutron interactions.

Neutron detection was further confirmed by analyzing the energy spectrum. Figure 3 presents the measured pulse height spectrum from the BGEM detector, superimposed with the simulation results. To account for the intrinsic energy resolution of the detector, a Gaussian smearing of 4% was applied to the simulated energy deposition. The simulation generally reproduces the characteristic features observed in the experimental spectrum. These results confirm that the detector is operating as expected.

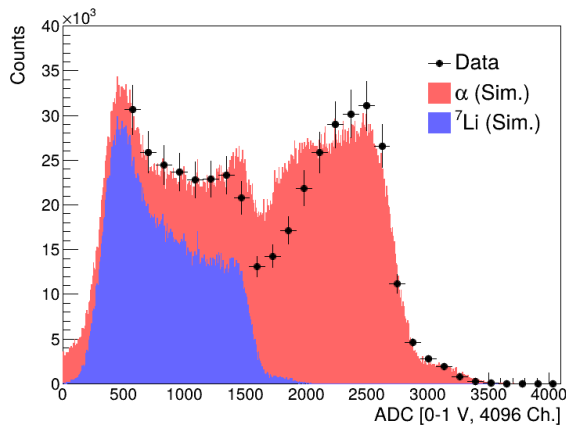


**Figure 3:** Pulse height spectrum measured with the BGEM detector. The simulation results corresponding to the energy deposition of  ${}^7\text{Li}$  ions and  $\alpha$  particles are overlaid as stacked filled histograms.

## 4.1 Detection Efficiency

To distinguish neutron signals from electronic noise and gamma-ray background, the count rates were measured as a function of the discriminator threshold at a fixed operating voltage of 4400 V. As summarized in Table 1, the background count rate (beam-off) decreases rapidly in the low-threshold region, dropping from 1265.0 Hz at 30 mV to 1.2 Hz at 60 mV. Above this value, the background rate becomes negligible. Consequently, a threshold of 60 mV was selected for the efficiency measurement, as it provides a sufficient rejection of noise events while maintaining a significant net neutron count rate of 200.0 Hz.

Based on this operating condition, the net count rates were measured to be 200.0 Hz for the BGEM and 2300 Hz for the reference LiCAF detector. Using Eq. 2 and assuming  $\epsilon_{\text{LiCAF}} \sim 1$ , the absolute cold neutron detection efficiency of the BGEM was calculated to be  $8.69 \pm 0.20\%$ . The reported uncertainty corresponds to the statistical error only.

This experimental result is in excellent agreement with the GEANT4 simulation of the detector geometry, which predicted a detection efficiency of 8.997% [9].

**Table 1:** Rate measurement results at 4400 V.

| Voltage | Threshold | Beam off (Hz) | Beam on (Hz) | On - Off |
|---------|-----------|---------------|--------------|----------|
| 4400 V  | 30        | 1265.0        | 1699.8       | 434.8    |
| 4400 V  | 40        | 124.6         | 352.9        | 228.3    |
| 4400 V  | 50        | 24.2          | 232.5        | 208.3    |
| 4400 V  | 60        | 1.2           | 201.2        | 200.0    |
| 4400 V  | 70        | 0.7           | 188.8        | 188.1    |

## 4.2 Imaging and Estimation of Spatial Resolution

The imaging capabilities and spatial resolution of the BGEM detector were evaluated using a cadmium (Cd) mask featuring 1 mm diameter holes. A

photograph of the mask and the corresponding reconstructed hit distribution are shown in Fig. 4. The individual hole peaks are clearly resolved in the selected region, allowing for a quantitative extraction of the spatial resolution.

Assuming a parallel incidence of the neutron beam, the spatial resolution was determined by analyzing the edge smearing of the reconstructed hole images. By fitting the radial edge profile with an error function, we obtained a spatial resolution of approximately  $700\ \mu\text{m}$ . It should be noted that if the incident neutron beam is not perfectly parallel, the beam divergence contributes to the broadening of the projected spots. Consequently, the intrinsic spatial resolution of the detector may be superior to the measured value presented here.

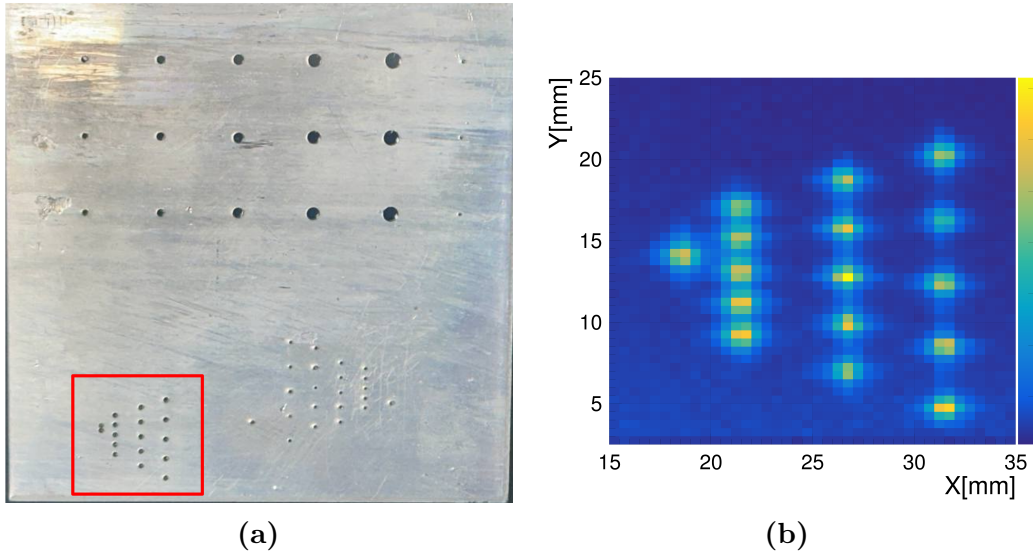


**Figure 4:** Cd-mask imaging used for the imaging and spatial-resolution measurement. (a) Photograph of the Cd hole mask with 1 mm diameter holes; the holes inside the red box were used for the spatial-resolution analysis. (b) Zoomed view of the reconstructed 2D hit-density map corresponding to the selected area.

## 5 Conclusion

We have developed a  $^{10}\text{B}$ -based GEM neutron detector featuring a  $^{10}\text{B}_4\text{C}$ -coated cathode and a 256-channel orthogonal strip readout system. The detector performance was evaluated at the HANARO Bio-REF cold neutron beamline, where it demonstrated stable operation with a distinct, beam-correlated neutron signal in the boron-coated configuration.

Using a calibrated Ce:LiCAF reference detector, the absolute neutron detection efficiency was measured to be  $8.69 \pm 0.20\%$  for 4.03 meV cold neutrons. In addition, spatial resolution tests performed with a Cd hole mask yielded a spatial resolution of approximately 700  $\mu\text{m}$ . These results validate the feasibility of BGEM technology as a practical,  $^3\text{He}$ -free solution for cold neutron beamline applications.

## Acknowledgments

This work was supported by the 2024 Research Fund of the University of Seoul (I. Park). This research was also supported by the National Research Foundation of Korea (NRF) grant funded by the Korea government (MSIT) (No. 2017R1A2B4006644) and by the Basic Science Research Program through the NRF funded by the Ministry of Education (No. 2018R1A6A1A06024977). We gratefully acknowledge Dr. Sangjin Jo and Dr. Myung-guk Moon of the Korea Atomic Energy Research Institute (KAERI) for their technical assistance with the  $\text{B}_4\text{C}$  coating on both the GEM and cathode foils, and for providing the neutron beam facility for this study.

## References

- [1] G.G. Daquino and W.P. Voorbraak. A review of the recommendations for the physical dosimetry of Boron Neutron Capture Therapy (BNCT). *OPOCE*, 2008.

- [2] J.B. Coble et al. Review of candidate techniques for material accountability measurements in electrochemical separations facilities. *Nuclear Technology*, 206(12):1803–1826, 2020.
- [3] R.T. Kouzes et al. Neutron detection alternatives to  $^3\text{He}$  for national security applications. *Nuclear Instruments and Methods in Physics Research Section A*, 623(3):1035–1045, 2010.
- [4] D.A. Brown et al. ENDF/B-VIII.0: The 8th major release of the nuclear reaction data library with CIELO-project cross sections, new standards and thermal scattering data. *Nuclear Data Sheets*, 148:1–142, 2018. Special Issue on Nuclear Reaction Data.
- [5] R.B. Firestone et al. Database of prompt gamma rays from slow neutron capture for elemental analysis. *IAEA*, 2004.
- [6] *Advances in Boron Neutron Capture Therapy*. International Atomic Energy Agency, Vienna, 2023.
- [7] F. Sauli. GEM: A new concept for electron amplification in gas detectors. *Nuclear Instruments and Methods in Physics Research Section A*, 386(2):531–534, 1997.
- [8] J. Allison et al. Recent developments in Geant4. *Nuclear Instruments and Methods in Physics Research Section A*, 835:186–225, 2016.
- [9] W. Kim et al. Study on structure of boron-based GEM detector for neutron with Geant4. *New Physics: Sae Mulli*, 75(7):536–542, 2025.
- [10] C. Höglund et al. B4C thin films for neutron detection. *Journal of Applied Physics*, 111(10):104908, 2012.
- [11] M. Abbas et al. Production and validation of industrially produced large-sized GEM foils for the Phase-2 upgrade of the CMS muon spectrometer. *Nuclear Instruments and Methods in Physics Research Section A*, 1057:168723, 2023.

- [12] M.J. French et al. Design and results from the APV25, a deep sub-micron CMOS front-end chip for the CMS tracker. *Nuclear Instruments and Methods in Physics Research Section A*, 466(2):359–365, 2001.
- [13] D. Choi et al. Bio-REF: Neutron reflectometer for investigation of bio-related thin films. *Physica B: Condensed Matter*, 551:236–243, 2018.
- [14] J. Iwanowska et al. Thermal neutron detection with  $\text{Ce}^{3+}$  doped  $\text{LiCaAlF}_6$  single crystals. *Nuclear Instruments and Methods in Physics Research Section A*, 652(1):319–322, 2011.